ACS APPLIED MATERIALS & INTERFACES

Research Article

www.acsami.org

Improved Performance of Photomultiplication Polymer Photodetectors by Adjustment of P3HT Molecular Arrangement

Wenbin Wang,[†] Fujun Zhang,*[,†] Lingliang Li,[†] Mile Gao,[†] and Bin Hu*[,†,‡]

[†]Key Laboratory of Luminescence and Optical Information, Ministry of Education, Beijing Jiaotong University, Beijing 100044, People's Republic of China

[‡]Department of Materials Science and Engineering, University of Tennessee, Knoxville, Tennessee 37996, United States

Supporting Information

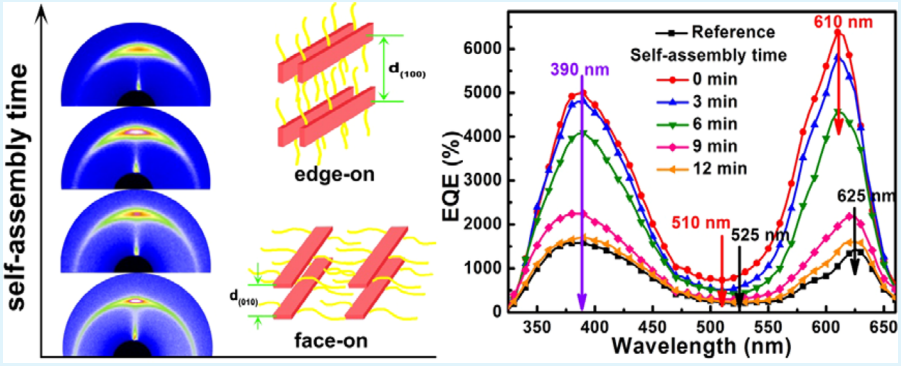

ABSTRACT: A series of photomultiplication (PM)-type polymer photodetectors (PPDs) were fabricated with polymer poly(3-hexylthiophene)−[6,6]-phenyl-C_{71}-butyric acid methyl ester (P3HT−$PC_{71}BM$) (100:1, w/w) as the active layers, the only difference being the self-assembly time of the active layers for adjusting the P3HT molecular arrangement. The grazing incidence X-ray diffraction (GIXRD) results exhibit that P3HT molecular arrangement can be adjusted between face-on and edge-on structures by controlling the self-assembly time. The champion EQE value of PPDs, based on the active layers without the self-assembly process, arrives at 6380% under 610 nm light illumination at −10 V bias, corresponding to the face-on molecular arrangement of P3HT in the active layers. The EQE values of PPDs were markedly decreased to 1600%, along with the self-assembly time up to 12 min, which should be attributed to the variation of absorption and hole transport ability of the active layers induced by the change of P3HT molecular arrangement. This finding provides an effective strategy for improving the performance of PM-type PPDs by adjusting the molecular arrangement, in addition to the enhanced trap-assisted charge-carrier tunneling injection.

KEYWORDS: *polymer photodetectors, photomultiplication, self-assembly, tunneling injection, mobility*

INTRODUCTION

Polymer photodetectors (PPDs) have attracted significant attention due to the rapid development of semiconducting polymers or small molecular materials that exhibit some advantages such as having a low cost of fabrication and being flexible, environmentally friendly, and lighter weight compared to their inorganic counterparts.[1−3] Up until now, most of the reported PPDs are photodiode-type photodetectors with external quantum efficiency (EQE) values less than unity and relatively fast response speeds.[4−6] The relatively low EQE values of photodiode-type PPDs is determined by the limited photon-harvesting efficiency, exciton dissociation efficiency, and charge-carrier transport and collection efficiency.[7−9] Therefore, the potential application of photodiode-type PPDs may be limited due to the relatively weak response. Highly sensitive photodetectors are desirable in a wide array of fields such as image sensing, communications, and environmental monitoring.[10−12] For highly sensitive photodetectors, high EQE values and low dark current are required to meet the various applications' needs. Photomultiplication (PM)-type photodetectors have attracted much attention due to their high EQE, which is defined by the number of charge carriers flowing across the photodetectors per incident photon.[13,14] The inorganic photomultiplier tubes and avalanche photodiodes exhibit high EQE values (larger than 100%), which are typically fabricated through impact ionization triggered by hot carriers, photoelectron-emission effect, or the secondary emission of electrons under the rather high bias (>100 V).[15,16] However, the charge carriers in organic materials are localized in single molecules due to their large binding energy and disordered structure, leading to the absence of hot carriers.[17,18]

Received: August 14, 2015
Accepted: September 25, 2015
Published: September 25, 2015

DOI: 10.1021/acsami.5b07522
ACS Appl. Mater. Interfaces 2015, 7, 22660−22668

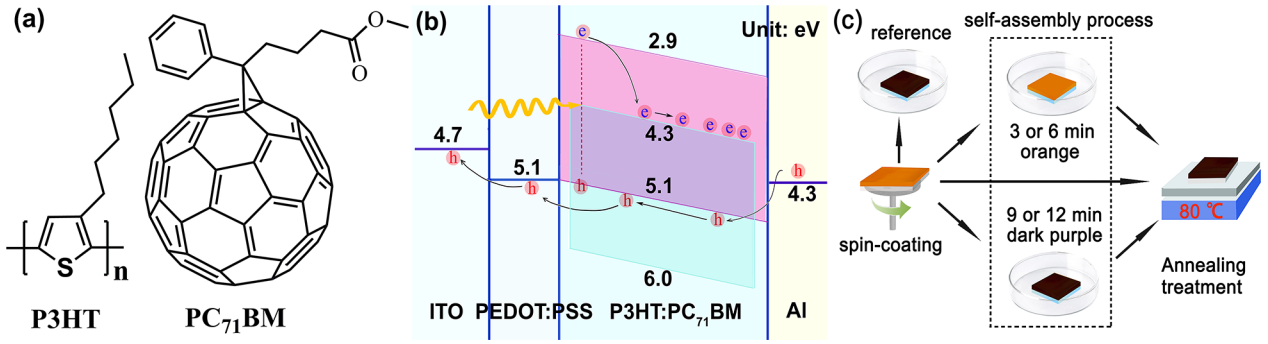

Figure 1. (a) The chemical structures of used materials, (b) the energy level alignment of used materials, and (c) the schematic diagram of controlling self-assembly process of the active layers.

To obtain the PM phenomenon in PPDs, photogenerated carriers should be trapped or blocked near the interface between the active layers and the electrode, while the opposite carriers can be injected from one electrode into the active layers and then effectively collected by the other electrode. Hiramoto et al. reported an EQE of 5000% under a relatively high bias of −20 V in perylene pigment film sandwiched between Au electrodes, and the PM phenomenon is attributed to the electron injection from the Au electrode to the perylene film assisted by the accumulation of photogenerated holes near the Au−perylene interface.[19] Hammond et al. also reported PM-type photodetectors based on NTCDA−C60 as hole-blocking layers, and the accumulated photogenerated holes near the ITO electrode can assist the strong electron injection leading to the PM phenomenon.[20] Chen et al. successfully achieved PM-type photodetectors based on inorganic nanoparticles; with CdTe doped into polymer poly(3-hexylthiophene)−[6,6]-phenyl-C_{71}-butyric acid methyl ester (P3HT−PC_{61}BM) (1:1, w/w) as the active layer, the maximum EQE value of 8000% was obtained under 350 nm light illumination, which is attributed to the enhanced hole-tunneling injection assisted by the trapped electrons in CdTe nanoparticles.[21] Recently, we first reported PM-type PPDs based on a (ITO−PEDOT:PSS−(P3HT−PC_{71}BM) (100:1, w/w)−LiF−Al) device structure, with the rather low PC_{71}BM content leading to the limited electron transport in the active layers.[22] The maximum EQE of 16 700% was obtained under −19 V bias, which is attributed to the enhanced hole tunneling injection assisted by trapped electrons in PC_{71}BM near Al cathode. It is interesting that the maximum EQE value was markedly increased to 37 500% only by removing the LiF interfacial layer, which further demonstrates that the trapped electrons in PC_{71}BM near Al cathode plays the key role in assisting hole tunneling injection from Al cathode into the active layers.[23] The EQE of PM-type PPDs should be co-determined by the trap-assisted hole-tunneling injection and hole transport ability in the P3HT−PC_{71}BM (100:1) active layers. The trap-assisted hole-tunneling injection is enhanced by removing the LiF interfacial layer, and the removal of the LiF interfacial layer can effectively decrease the width of hole-injection barrier for the enhanced hole tunneling injection.[23] It is known that charge-transport ability in the active layers should be strongly determined by the molecular arrangement, which has been widely reported in organic solar cells (OSCs) and organic thin film transistors (OTFT).[24−26] As we know, the main P3HT molecular arrangement are the $\pi-\pi$ stacking direction parallel to the substrate, and with the alkyl side chains' direction perpendicular to the substrate (edge-on) or with the alkyl side chains' direction parallel to the substrate (face-on), the different molecular arrangement strongly influences the hole transport ability in the active layers.[27,28] The edge-on molecular arrangement is beneficial for the hole transport along the direction parallel to the substrate, such as in the lateral-structure OTFTs. The high charge transport ability should be desired along the direction perpendicular to substrate for the sandwiched structure devices, such as OSCs and PPDs. The face-on molecular arrangement of P3HT in the active layers should be beneficial to hole transport along the $\pi-\pi$ stacking direction perpendicular to substrate for further performance improvement of the PM type PPDs.

In this study, a series of PM-type PPDs were fabricated based on P3HT−PC_{71}BM (100:1, w/w) as the active layers, the only difference being the self-assembly time of the active layers for adjusting the P3HT molecular arrangement. The EQE values of the PM type PPDs are markedly increased by shortening the self-assembly time of the active layers. The champion EQE value of 6380% was obtained on the basis of the active layers without the self-assembly process under 610 nm light illumination at −10 V bias. The EQE enhancement is mainly attributed to the increased hole transport ability induced by P3HT face-on molecular arrangement in the active layers. The variation of EQE spectral shape and EQE values of the PM type PPDs was investigated from the absorption spectra and the photogenerated electron-distribution dependence on the self-assembly time of the active layers.

EXPERIMENTAL SECTION

The indium tin oxide (ITO)-coated glass substrates, with a sheet resistance of 15 Ω per square, were sequentially cleaned by ultrasonic treatment in detergent, deionized water, and ethanol. The cleaned ITO substrates were dried by nitrogen gas and treated by UV ozone for 10 min to increase the work function of the ITO surface. The solution of PEDOT:PSS was spin-coated onto the cleaned ITO substrates at a spin speed of 5000 rounds per minute (rpm) for 40 s. The PEDOT:PSS-coated ITO substrates were baked at 120 °C for 10 min. Polymer poly(3-hexylthiophene) (purchased from Nichem Fino Technology Co., Ltd.) and [6,6]-phenyl-C_{71}-butyric acid methyl ester (purchased from Luminescence Technology Corp.) were dissolved in 1,2-dichlorobenzene (*o*-DCB) to prepare 40 mg/mL solutions, respectively. The molecular weight and regioregularity of the used P3HT is about 48 000 g/mol and between 91 and ~94%, respectively. The mixed P3HT−PC_{71}BM solution was then prepared with P3HT−PC_{71}BM weight ratio as 100:1. The mixed solution was spin-coated onto a PEDOT:PSS layer at 800 rpm for 30 s in a high-nitrogen-filled glovebox. The wet active layers were allowed to sit for different times (0, 3, 6, 9, or 12 min) for molecular self-assembly before annealing treatment at 80 °C for 20 s, which provides an opportunity for the P3HT molecular self-assembly process in the wet films. The 100 nm

DOI: 10.1021/acsami.5b07522
ACS Appl. Mater. Interfaces 2015, 7, 22660−22668

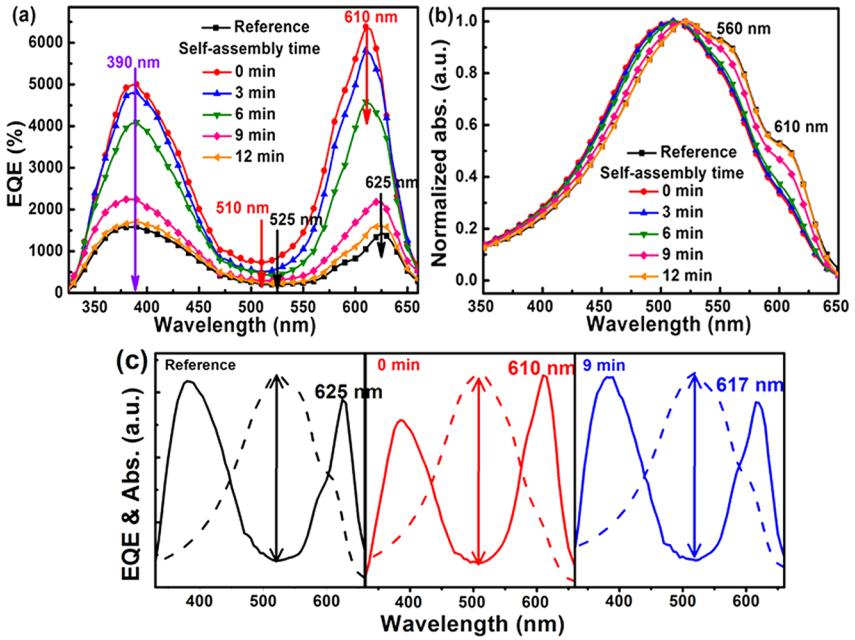

Figure 2. (a) EQE spectra of all PPDs with different self-assembly time under a −10 V bias, (b) normalized absorption spectra of active layers with different self-assembly process, and (c) the comparison between the EQE spectrum of PPDs and the absorption spectrum of the corresponding active layer.

aluminum layer was thermally evaporated on the active layers in a high vacuum (10^{-4} pa) chamber. The active area of each device is about 3.8 mm^2, which is defined by the vertical overlap of the Al cathode and ITO anode. The chemical structures of the used materials and the schematic energy level diagram of device are shown in parts a and b of Figure 1, respectively. The schematic diagram of the self-assembly process of active layers is shown in Figure 1c.

The current density versus voltage (J–V) curves of PPDs were measured by a Keithley 2400 source meter under 625 nm light illumination with an intensity of 8.87 $\mu W/cm^2$. The used monochromatic light was provided by a 150 W xenon lamp coupled with a monochromator. The monochromatic light intensity and wavelength were monitored and calibrated by a Newport 818-UV power meter and an Acton SpectraPro 2150i CCD spectrometer. The absorption spectra of the active layers were measured by a Shimadzu UV-3101 PC spectrophotometer. The thickness of active layers was measured by an Ambios Technology XP-2 stylus profilometer. Grazing incidence X-ray diffraction (GIXRD) images were measured by a five-circle Huber diffractometer at the Beijing Synchrotron Radiation Facility (BSRF). A bent-triangle silicon crystal was used to select the X-rays of a wavelength of 1.5476 Å. A grazing incidence angle of 0.4° was chosen to increase GIXRD peak intensity for investigating the crystallinity and orientation that prevailed throughout the film. All of the measurements were carried out at room temperature in the ambient conditions.

RESULTS AND DISCUSSION

A series of solution-processed PPDs with P3HT−$PC_{71}BM$ (100:1, w/w) as the active layers were fabricated to investigate the effect of P3HT molecular arrangement on the performance of PPDs. The only difference is the self-assembly time of the active layers before annealing treatment. The self-assembly time was defined as the time interval between the spin-coating stopping and the annealing treatment starting. The self-assembly process should play a key role in determining P3HT molecular arrangement in the active layers. The self-assembly time of active layers can be adjusted in the relatively large scale up to 12 min due to the high boiling point (180 °C) of o-DCB solvent.[29,30] The color of the active layers changed from orange to dark purple along with the increase of self-assembly time, as shown in Figure 1c. The active layers were directly annealed at 80 °C after spin-coating, defined as without the self-assembly process. For the reference PPDs, the active layers were not suffered from annealing treatment. To clarify the effect of the self-assembly process and the annealing treatment on the performance of PPDs, we measured the EQE spectra of all PPDs, and they are shown in Figure 2a. It is apparent that the EQE values of all PPDs are much larger than 100% in the spectral range from 350 to 650 nm at −10 V bias, exhibiting an apparent PM phenomenon.

The working mechanism of PM-type PPDs is attributed to interfacial trap-assisted hole-tunneling injection.[22,23,31] As we can envision, most of the incident photons with wavelengths from 450 to 570 nm can be effectively harvested by P3HT according to its absorption spectrum, resulting in most of the excitons or electrons generated near the ITO anode. The photogenerated electrons will be trapped in $PC_{71}BM$ molecules surrounded by P3HT due to the 1.4 eV LUMOs barrier difference between P3HT and $PC_{71}BM$. The fewer photogenerated electrons can be accumulated in $PC_{71}BM$ near the Al cathode due to the absent electron transport channels in the active layers with rather low $PC_{71}BM$ content, which is the underlying reason for the apparent dip in the EQE spectra of PPDs. It is known that only the photogenerated electrons trapped in $PC_{71}BM$ near the Al cathode can induce the interfacial energy band bending to decrease the hole injection barrier width, which is beneficial to the enhanced hole-tunneling injection. It should be highlighted that an apparent peak at about 390 nm in the EQE spectra was observed for all PPDs, which should be attributed to the photon harvesting by $PC_{71}BM$ according to the absorption spectrum of the $PC_{71}BM$ film (shown in Figure S1). Meanwhile, another apparently shifted EQE peak was observed in the longer wavelength range, which should be related to the absorption intensity variation of P3HT induced by self-assembly time and annealing treatment on the active layers. The absorption spectra of active layers with

DOI: 10.1021/acsami.5b07522
ACS Appl. Mater. Interfaces 2015, 7, 22660−22668

different self-assembly time were measured to confirm the relationship between EQE spectra and corresponding absorption spectra. The normalized absorption spectra are shown in Figure 2b, which is beneficial for contrasting the EQE and absorption spectral shape for exhibiting their fine dependence. A similar shift of the absorption peak can be obviously observed for the active layers with different self-assembly time. The shoulder absorption peaks at 560 and 610 nm of P3HT become more and more apparent, along with increased self-assembly time of the active layers. It is known that the shoulder absorption peak at 560 nm is attributed to the absorption of extended conjugation lengths of P3HT in the solid state, and the shoulder absorption peak at 610 nm is related to the ordered interchain stacking of P3HT molecules.[32−34] The P3HT absorption spectral-shape dependence on molecular arrangement has been commonly reported in the PSCs with P3HT−$PC_{71}BM$ as the active layers.[35,36] To further intuitively exhibit the relationship between EQE and absorption spectral-shape dependence on the self-assembly time of the active layers, we depicted the corresponding EQE and absorption spectra together, as shown in Figure 2c. It is apparent that the EQE spectral valley well accords with its absorption spectral peak and the EQE spectral peaks locate at the position of relatively weak absorption intensity of the active layers. The exact matching between EQE spectral valley of PPDs and absorption spectral peak of active layers further demonstrates that the working mechanism of PM-type PPDs is completely different from that of PSCs. In fact, the EQE peaks of PPDs are the relative maximum values in the corresponding spectral range, which is strongly determined by the number of trapped electrons in $PC_{71}BM$ near the Al cathode.

Another interesting phenomenon that should be highlighted that the EQE values of PPDs are increased by shortening the self-assembly time, as shown in Figure 2a. For the active layers with 12 min self-assembly, the corresponding PPDs exhibit slightly large EQE values compared with that of the reference PPDs without annealing treatment. For the active layers without self-assembly process (annealing treatment after spin-coating), the PPDs exhibit the champion EQE values in the whole spectral range. The detailed EQE peak positions and values of PPDs with different self-assembly times of the active layers are listed in Table 1. The maximum EQE values of PPDs

Table 1. Detailed EQE peaks and EQE Values of All PPDs under −10 V Bias

SAT (min)	EQE peak (nm)	EQE (%)	EQE peak (nm)	EQE (%)	ratio
0	390	5000	610	6380	1.28
3	390	4810	610	5820	1.21
6	390	4090	610	4580	1.09
9	390	2240	620	2200	0.98
12	390	1710	622	1600	0.94
ref	390	1590	625	1440	0.91

SAT, self-assembly time; ref, active layer without annealing treatment.

in the longer wavelength range were decreased from 6380% to 1600%, along with the increase of self-assembly time, and to 1440% for the reference devices under −10 V bias, along with the EQE peak red-shift from 610 to 625 nm. The EQE values at 390 nm were decreased from 5000% to 1710%, along with the increase of self-assembly time, and to 1590% for the reference devices under −10 V bias. It is apparent that the ratios of the maximum EQE value in longer wavelength ranges to the EQE value at 390 nm were decreased from 1.28 to 0.94, along with the self-assembly time up to 12 min, and to 0.91 for the reference devices. On the basis of the working mechanism of PM-type PPDs, the EQE values should be co-determined by hole-tunneling injection and hole transport ability in the corresponding active layers. The hole-tunneling injection should be determined by the number of trapped electrons in $PC_{71}BM$ near Al cathode.[23] The photogenerated electron distribution in the active layers strongly depends on the absorption coefficient of the blend films with different self-assembly time. The hole transport ability of blend films is mainly determined by the P3HT molecular arrangement in the active layers.

It is known that P3HT molecular arrangement can be adjusted by controlling self-assembly time, which can be confirmed from the absorption spectra of the P3HT−$PC_{71}BM$ (100:1) blend films with different self-assembly times, as shown in Figure 3a. A series of blend films were fabricated under the same conditions, with the only difference being the self-assembly time. It is apparent that the absorption intensity of active layers was kept almost constant in the shorter wavelength range. However, the absorption intensity of active layers was decreased in the longer wavelength range, along with the decrease of self-assembly time. The decreased absorption intensity in the longer wavelength range is beneficial to the greater number of excitons or electrons generated in $PC_{71}BM$ near Al cathode, which can be further demonstrated from the photogenerated electrons distribution in the active layers. As we can envision, $PC_{71}BM$ molecules may be uniformly dispersed in the active layers due to the rather low $PC_{71}BM$ content in the active layers. The vertical phase separation should be neglected due to the rather low content, especial for the active layers with short self-assembly processes. Therefore, the exciton dissociation efficiency can be considered as the same in the whole active layers due to the homogeneous distribution of $PC_{71}BM$. The optical-field distribution in the all PPDs can be calculated according to the absorption coefficient of active layers,[37] as shown in Figure S2. Assuming the same exciton dissociation efficiency in the whole active layers, the photogenerated electron distributions in the active layers were calculated according to the optical-field distribution, as shown in Figure S3. The typical photogenerated electron distributions of the PPDs without annealing treatment or without self-assembly are shown in panels b and c of Figure 3, respectively. The dark color in the photogenerated electrons distribution image indicates the large electron density in this zone. It is apparent that the number of photogenerated electrons near the Al cathode in the active layers without self-assembly is much larger than that in the active layers without annealing treatment in the longer wavelength range, as marked by red circles in Figure 3b,c. As we know, the number of trapped electrons in $PC_{71}BM$ near the Al cathode plays the key role in determining the hole-tunneling injection from the Al cathode into the active layers. The photogenerated electrons distributions on the cross-section, about 20 nm from the Al cathode, are depicted in Figure 3d. It is apparent that the photogenerated electron density in the short wavelength range was kept almost constant for the active layers with different self-assembly times, while in the longer wavelength range, the photogenerated electron density was increased along with the decrease of self-assembly time, which can well support the enhanced EQE values of the corresponding PPDs. Meanwhile, the photogenerated electron

DOI: 10.1021/acsami.5b07522
ACS Appl. Mater. Interfaces 2015, 7, 22660−22668

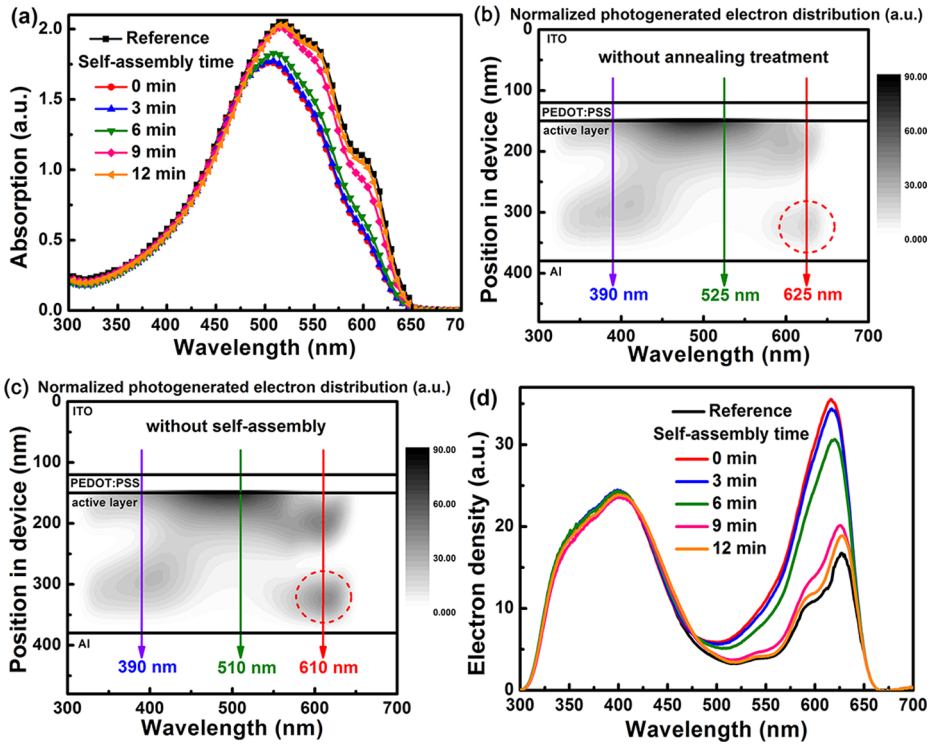

Figure 3. (a) Absorption spectra of blend films with different self-assembly times, (b) photogenerated electron distribution in the active layers of the reference PPDs, (c) photogenerated electron distribution in the active layers of the PPDs without the self-assembly process, and (d) the cross-section photogenerated electron distribution in the active layers about 20 nm from the Al cathode.

distribution on this cross-section is very similar to the EQE spectral shape of PPDs, which further demonstrates that the EQE values of PPDs are strongly determined by the number of trapped electrons in $PC_{71}BM$ near the Al cathode.

To clarify the effect of P3HT molecular arrangement on hole transport ability in the active layers, we fabricated the hole-only devices (ITO−PEDOT:PSS−active layers−MoO_3 (10 nm)−Ag (100 nm)) based on the active layers with different self-assembly times. The space-charge-limited current (SCLC) model was employed to investigate the hole transport properties of the active layers with different self-assembly time.[38,39] The $J^{1/2}-V$ curves of hole-only devices were measured in dark conditions and are shown in Figure 4. It is apparent that the hole transport ability is increased along with the decreased self-assembly time of the active layers. Therefore,

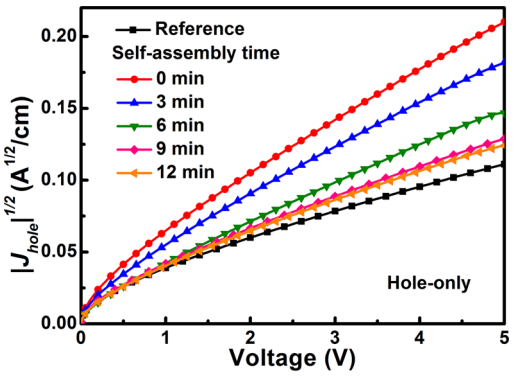

Figure 4. $J^{1/2}-V$ curves of hole-only devices (ITO−PEDOT:PSS−(P3HT−$PC_{71}BM$) (100:1, w/w)−MoO_3−Ag) with different self-assembly times of active layers.

the EQE values of PPD dependence on hole transport ability in the active layers can be well-explained according to the following equation:

$$\mathrm{EQE} = \frac{\chi\tau}{T} = \frac{\chi\tau\mu V}{L^2} \quad (1)$$

where χ is the fraction of excitons that dissociate into trapped electrons and free holes, τ is the lifetime of the trapped electron, T is the hole transport time, V is the applied bias, L is the active layer thickness, and μ is the hole transport ability.[40] It is apparent that the EQE is proportional to the hole transport ability of the active layers. As we know, the EQE values of the PPDs are codetermined by the hole-tunneling injection and hole transport ability in the corresponding active layers. On the basis of the EQE spectra of all PPDs and the photogenerated electron distributions of the cross-section near the Al cathode, shown in Figures 2a and 3d, we determined that the enhanced EQE values in the short wavelength range are mainly determined by the improved hole-transport ability in the active layers, while in the longer wavelength range, the enhanced EQE values are codetermined by the enhanced hole-tunneling injection and the improved hole transport ability of active layers. The enhanced hole-tunneling injection can be confirmed from the more photogenerated electrons distribution in $PC_{71}BM$ near the Al cathode for the active layers with the shorter self-assembly time.

To further confirm the effect of self-assembly time on the EQE values of PPDs, we measured the current density−voltage curves of all PPDs in dark or under 625 nm light illumination with an intensity of 8.87 $\mu W/cm^2$, as shown in Figure 5a,b. It is apparent that the dark current density of all PPDs was rather low and kept almost constant for all PPDs due to the limited hole injection in the dark conditions. The light current density

DOI: 10.1021/acsami.5b07522
ACS Appl. Mater. Interfaces 2015, 7, 22660−22668

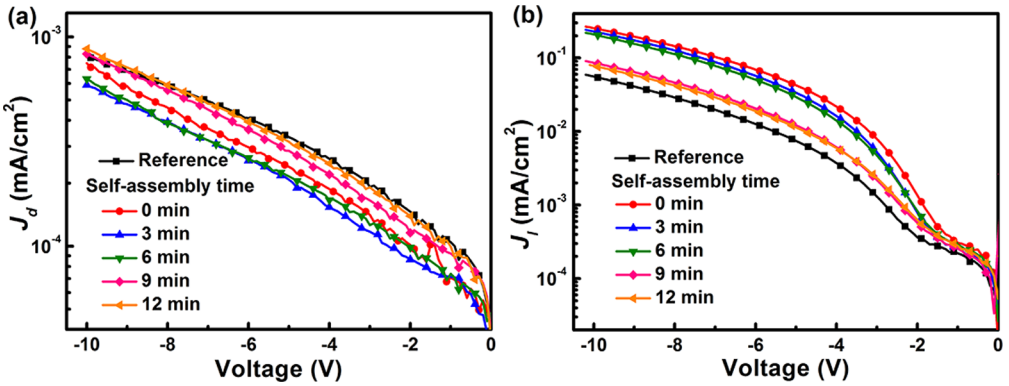

Figure 5. J–V curves of the all PPDs (a) in dark conditions and (b) under 625 nm light illumination with an intensity of 8.87 μW/cm^2.

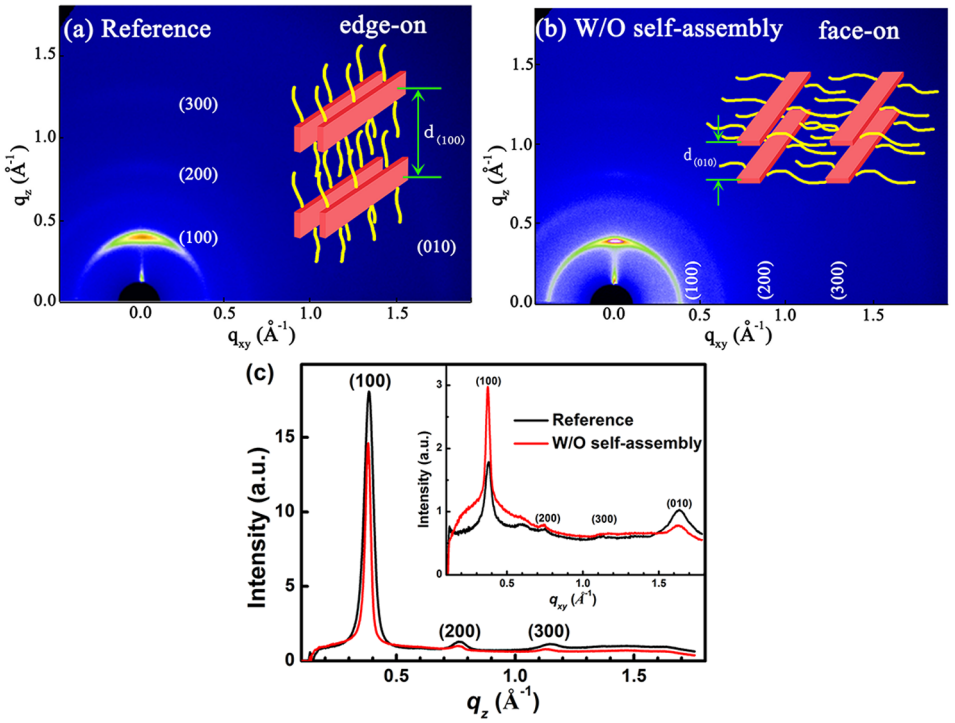

Figure 6. 2D GIXRD patterns of the films: (a) active layers without annealing treatment, (b) active layers without the self-assembly process, and (c) 1D OOP XRD profiles of two kinds of active layers. The inset shows the corresponding 1D IP XRD profiles.

of the PPDs is 2 orders of magnitude larger than the dark current density under −10 V bias and the rather weak light intensity of 8.87 μW/cm^2. The light current density was increased along with the decreased self-assembly time of the active layers, which well-accords with the EQE value dependence on the self-assembly time of the active layers. The increased light current density should be attributed to the enhanced hole-tunneling injection and hole transport ability in the active layers.

According to the above experimental results, the absorption spectral shape, relative absorption intensity, and hole transport ability of active layers should be determined by P3HT molecular arrangement, which can be adjusted by the self-assembly time of active layers. To clarify the underlying reason, we investigated the P3HT molecular-arrangement dependence on the self-assembly time of the active layers by grazing incidence X-ray diffraction.[41] The two-dimensional (2D) GIXRD patterns of all the active layers are shown in Figure S4. The typical 2D GIXRD patterns of active layers without annealing treatment and without self-assembly are shown in Figure 6a,b. The 1D out-of-plane (OOP) and in-plane (IP) X-ray diffraction profiles (diffraction vector q = 0.38, 0.76, and 1.14 Å^{-1} for the primary (100), secondary (200), and tertiary (300) peaks, respectively) can be extracted from the 2D GIXRD patterns, as shown in Figure 6c and its inserted image, respectively. The intense reflections of the (h00) plane along the q_z (out-of-plane) and a relative weak (010) plane along q_{xy} (in-plane) axes of the active layers without annealing treatment can be observed from Figure 6a, which implies that P3HT molecules would favor having an edge-on structure on the substrate, i.e., hexyl side-chains perpendicular to the substrate and the π–π stacking direction of P3HT backbones parallel to the substrate.[42−44] The P3HT molecules prefer to form the more thermodynamically favorable edge-on structure during the long self-assembly process of active layers without annealing treatment. The relative reflection intensity of (h00) and (010) planes can be confirmed from the 1D XRD patterns. For the active layers without the self-assembly process, intense

DOI: 10.1021/acsami.5b07522
ACS Appl. Mater. Interfaces 2015, 7, 22660−22668

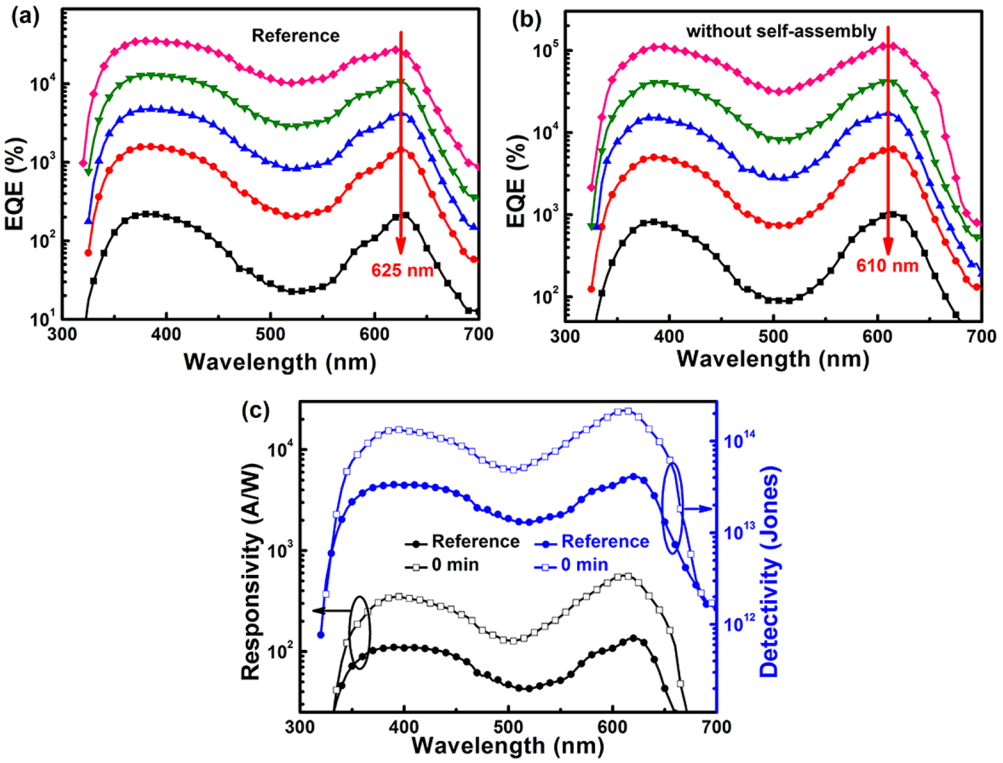

Figure 7. EQE spectra of the PM-type PPDs under different biases from −7 to −19 V with an interval of 3 V: (a) reference PPDs, (b) PPDs without the self-assembly process, and (c) the corresponding responsivity and detectivity of the PPD dependence on illumination light wavelength under a −19 V bias.

reflections of the $(h00)$ plane along both q_z and q_{xy} axes can be observed from the Figure 6b. The thermodynamically stable edge-on crystal structure cannot be sufficiently developed from coil-like P3HT in the active layer by direct annealing treatment without the self-assembly process. It means that the P3HT molecules prefer to have the mixed conformations including edge-on and face-on structures on the substrate. According to the Figure 6c, the OOP $(h00)$ peak intensity of the active layers without the self-assembly process is lower than that of the reference films, indicating a relatively low crystallinity degree.[43] As seen from the inset of Figure 6c, the IP $(h00)$ peak intensity of the active layers without the self-assembly process is higher than that of the reference films, and the IP (010) peak intensity of the active layers without the self-assembly process is lower than that of the reference films. This result further indicates that the ordered face-on structure of P3HT molecules prefers to be formed in the active layers without the self-assembly process.[27,44,45] The face-on structure in P3HT molecules is beneficial to hole transport along the direction perpendicular to the substrate.[46] The experimental results provide the more convincing evidence to explain the enhanced hole transport ability along the direction perpendicular to the substrate for the active layer with shorted self-assembly time.

It is known that the charge carrier transport ability in the active layers should be enhanced along with the increase of bias applied on the device. To further confirm EQE values of PPD dependence on the hole transport ability in the active layers, we measured the EQE spectra of all PPDs under different bias from −7 to −19 V with an interval of 3 V and are shown in Figure S5. The EQE spectra of the typical PPDs under different bias are shown in Figure 7a,b. It is apparent that the EQE values of all PPDs are rapidly increased along with the increase of applied bias, which can be well-explained from the enhanced hole-tunneling injection and hole transport ability along with the increase of applied bias. As we know, the energy level of P3HT should be more tilted under the higher bias, which can further decrease the width of hole tunneling barrier from Al cathode into the active layers for the better hole tunneling injection. In addition, hole transport ability in the active layers should be improved under the higher bias, resulting in the shorted hole transport time (T) for passing through the whole active layer according to the eq 1. The highest EQE values of the reference PPDs at 390 and 625 nm are 35 100% and 26 500% under −19 V bias, respectively. For the PPDs without self-assembly process, the highest EQE values at 390 and 610 nm are 110 700% and 115 800% under −19 V bias, respectively.

The responsivity (R) and detectivity (D^*) values of the PPD dependence on wavelength were calculated according to the EQE values of the PPDs and light intensity spectrum of the monochromatic light, as shown in Figure 7c. The light-intensity spectrum of the monochromatic light is shown in Figure S6. It is apparent that the R and D^* of PPDs without the self-assembly process are much larger than those of the reference PPDs. The detailed EQE, R, and D^* values of the PM-type PPDs are summarized in Table 2. The calculation of R is expressed in the following equation:

$$R = \frac{J_{ph}}{I_{in}} \tag{2}$$

where J_{ph} is the photocurrent density, and I_{in} is the incident light intensity. The incident light intensity is 13.02, 9.12, or 8.87 $\mu W/cm^2$ corresponding to 390, 610, or 625 nm, respectively. The D^* is calculated according to the following equation:[6,47]

DOI: 10.1021/acsami.5b07522
ACS Appl. Mater. Interfaces 2015, 7, 22660−22668

Table 2. Key Parameters of the Two Typical PPDs under the Given Conditions

SAT (min)	λ (nm)	intensity (μW/cm²)	EQE (%)	R (A/W)	D* (Jones)
ref	390	13.00	35 100	110.2	3.35×10^{13}
	625	8.87	26 500	133.2	4.04×10^{13}
0 min	390	13.00	110 700	347.5	1.32×10^{14}
	610	9.12	115 800	568.6	2.17×10^{14}

SAT, self-assembly time; ref, active layer without annealing treatment.

$$D^* = \frac{R}{(2eJ_d)^{1/2}} \quad (3)$$

where J_d is the dark current density, and e is the absolute value of the electron charge (1.6×10^{-19} coulomb). For the reference PPDs, the champion R and D^* values are 133.2 A/W and 4.04×10^{13} Jones under 625 nm light illumination under −19 V bias, respectively. For the PPDs without self-assembly process, the champion R and D^* values arrive to 568.6 A/W and 2.17×10^{14} Jones under 610 nm light illumination under −19 V bias, respectively. The enhanced R and D^* of PPDs without self-assembly process should be mainly attributed to the increased hole transport ability in the active layer, with P3HT having the face-on oriented molecular arrangement. Meanwhile, the rather high R and D^* values should be attributed to the relatively low dark current due to the large hole-injection barrier of 0.8 eV between the Fermi level of Al and the HOMO of P3HT. The electron current can be neglected due to the rather low $PC_{71}BM$ doping ratio in the active layers leading to the absence of electron-transporting channels.

CONCLUSIONS

In summary, the EQE values of PM-type PPDs are markedly increased by adjusting P3HT molecular arrangement. The champion EQE value of PPDs based on the active layers without the self-assembly process arrives at 6380% under 610 nm light illumination at −10 V bias. The fine match spectral shape between the absorption of active layers and the EQE of the corresponding PPDs demonstrates that the PM phenomenon of PPDs is attributed to the enhanced hole-tunneling injection assisted by the trapped electrons in $PC_{71}BM$ near Al cathode. The photogenerated electrons distribution in the active layer further demonstrate that the number of trapped electrons in $PC_{71}BM$ near the Al cathode plays the key role in the hole-tunneling injection under reverse bias. The GIXRD experimental results provide solid and direct evidence on the P3HT molecular arrangement induced by the self-assembly time. The P3HT molecular arrangement not only influences its absorption but also the hole transport ability along the direction perpendicular to the substrate. The face-on oriented P3HT molecular arrangement is beneficial to hole transport along the direction perpendicular to the substrate. The molecular arrangement should play an important role in determining the performance of organic electronic devices.

ASSOCIATED CONTENT

Supporting Information

The Supporting Information is available free of charge on the ACS Publications website at DOI: 10.1021/acsami.5b07522.

Absorption spectrum of $PC_{71}BM$ film. Additional information on and images showing the optical field distribution of the all PPDs; the photogenerated electron distributions in the active layers; the simulated optical field distribution; the 2D GIXRD patterns of all the active layers; the EQE spectra of the PPDs based on the active layers with 3, 6, 9, and 12 min self-assembly; and the light intensity spectrum of the monochromatic lights through a monochromator. (PDF)

AUTHOR INFORMATION

Corresponding Authors

*E-mail: fjzhang@bjtu.edu.cn

*E-mail: bhu@utk.edu. Tel: 0086-10-51684908.

Notes

The authors declare no competing financial interest.

ACKNOWLEDGMENTS

This work was supported by Fundamental Research Funds for the Central Universities (2014JBZ017), the National Natural Science Foundation of China (61377029), the Beijing Natural Science Foundation (2122050), and the Beijing Synchrotron Radiation Facility (BSRF) of the Institute of High Energy, Chinese Academy of Science.

REFERENCES

(1) Dong, H. L.; Zhu, H. F.; Meng, Q.; Gong, X.; Hu, W. P. Organic Photoresponse Materials and Devices. *Chem. Soc. Rev.* **2012**, *41*, 1754−1808.

(2) Baeg, K. J.; Binda, M.; Natali, D.; Caironi, M.; Noh, Y. Y. Organic Light Detectors: Photodiodes and Phototransistors. *Adv. Mater.* **2013**, *25*, 4267−4295.

(3) Rauch, T.; Boberl, M.; Tedde, S. F.; Furst, J.; Kovalenko, M. V.; Hesser, G. N.; Lemmer, U.; Heiss, W.; Hayden, O. Near-Infrared Imaging with Quantum-Dot-Sensitized Organic Photodiodes. *Nat. Photonics* **2009**, *3*, 332−336.

(4) Su, Z. S.; Hou, F. H.; Wang, X.; Gao, Y.; Jin, F. M.; Zhang, G.; Li, Y. T.; Zhang, L. G.; Chu, B.; Li, W. L. High-Performance Organic Small-Molecule Panchromatic Photodetectors. *ACS Appl. Mater. Interfaces* **2015**, *7*, 2529−2534.

(5) Li, L. L.; Zhang, F. J.; An, Q. S.; Wang, Z. X.; Wang, J.; Tang, A. W.; Peng, H. S.; Xu, Z.; Wang, Y. S. Organic Ultraviolet Photodetector Based on Phosphorescent Material. *Opt. Lett.* **2013**, *38*, 3823−3826.

(6) Gong, X.; Tong, M. H.; Xia, Y. J.; Cai, W. Z.; Moon, J. S.; Cao, Y.; Yu, G.; Shieh, C. L.; Nilsson, B.; Heeger, A. J. High-Detectivity Polymer Photodetectors with Spectral Response from 300 to 1450 nm. *Science* **2009**, *325*, 1665−1667.

(7) Lee, H.; Nam, S.; Kwon, H.; Lee, S.; Kim, J.; Lee, W.; Lee, C.; Jeong, J.; Kim, H.; Shin, T. J.; Kim, Y. Solution-Processable All-Small Molecular Bulk HeterojunctionFilms for Stable Organic Ohotodetectors: Near UV and Visible Light Sensing. *J. Mater. Chem. C* **2015**, *3*, 1513−1520.

(8) Lin, H. W.; Ku, S. Y.; Su, H. C.; Huang, C. W.; Lin, Y. T.; Wong, K. T.; Wu, C. C. Highly Efficient Visible-Blind Organic Ultraviolet Photodetectors. *Adv. Mater.* **2005**, *17*, 2489−2493.

(9) Baierl, D.; Pancheri, L.; Schmidt, M.; Stoppa, D.; Dalla Betta, G. F.; Scarpa, G.; Lugli, P. A Hybrid CMOS-Imager with a Solution-Processable Polymer as Photoactive Layer. *Nat. Commun.* **2012**, *3*, 1175.

(10) Konstantatos, G.; Sargent, E. H. Nanostructured Materials for Photon Detection. *Nat. Nanotechnol.* **2010**, *5*, 391−400.

(11) Chen, F. C.; Chien, S. C.; Cious, G. L. Highly Sensitive, Low-voltage, Organic Photomultiple Photodetectors Exhibiting Broadband Response. *Appl. Phys. Lett.* **2010**, *97*, 103301.

(12) Lee, J. W.; Kim, D. Y.; So, F. Unraveling the Gain Mechanism in High Performance Solution-Processed PbS Infrared PIN Photodiodes. *Adv. Funct. Mater.* **2015**, *25*, 1233−1238.

(13) Guo, F. W.; Yang, B.; Yuan, Y. B.; Xiao, Z. G.; Dong, Q. F.; Bi, Y.; Huang, J. S. A Nanocomposite Ultraviolet Photodetector Based on

DOI: 10.1021/acsami.5b07522
ACS Appl. Mater. Interfaces 2015, 7, 22660−22668

Interfacial Trap-Controlled Charge Injection. *Nat. Nanotechnol.* **2012**, *7*, 798−802.
(14) Saran, R.; Stolojan, V.; Curry, R. J. Ultrahigh Performance C60 Nanorod Large Area Flexible Photoconductor Devices via Ultralow Organic and Inorganic Photodoping. *Sci. Rep.* **2014**, *4*, 5041.
(15) Nevet, A.; Hayat, A.; Orenstein, M. Ultrafast Three-Photon Counting in a Photomultiplier Tube. *Opt. Lett.* **2011**, *36*, 725−727.
(16) Hayden, O.; Agarwal, R.; Lieber, C. M. Nanoscale Avalanche Photodiodes for Highly Sensitive and Spatially Resolved Photon Detection. *Nat. Mater.* **2006**, *5*, 352−356.
(17) Reynaert, J.; Arkhipov, V. I.; Heremans, P.; Poortmans, J. Photomultiplication in Disordered Unipolar Organic Materials. *Adv. Funct. Mater.* **2006**, *16*, 784−790.
(18) Pettersson, L. A. A.; Roman, L. S.; Inganäs, O. Quantum Efficiency of Exciton-to-Charge Generation in Organic Photovoltaic Devices. *J. Appl. Phys.* **2001**, *89*, 5564.
(19) Hiramoto, M.; Imahigashi, T.; Yokoyama, M. Photocurrent Multiplication in Organic Pigment Films. *Appl. Phys. Lett.* **1994**, *64*, 187−189.
(20) Hammond, W. T.; Xue, J. G. Organic Heterojunction Photodiodes Exhibiting Low Voltage, Imaging-Speed Photocurrent Gain. *Appl. Phys. Lett.* **2010**, *97*, 073302.
(21) Chen, H. Y.; Lo, M. K. F.; Yang, G. W.; Monbouquette, H. G.; Yang, Y. Nanoparticle-Assisted High Photoconductive Gain in Composites of Polymer and Fullerene. *Nat. Nanotechnol.* **2008**, *3*, 543−547.
(22) Li, L. L.; Zhang, F. J.; Wang, J.; An, Q. S.; Sun, Q. Q.; Wang, W. B.; Zhang, J.; Teng, F. Achieving EQE of 16,700% in P3HT: $PC_{71}BM$ Based Photodetectors by Trap-Assisted Photomultiplication. *Sci. Rep.* **2015**, *5*, 9181.
(23) Li, L. L.; Zhang, F. J.; Wang, W. B.; An, Q. S.; Wang, J.; Sun, Q. Q.; Zhang, M. Trap-Assisted Photomultiplication Polymer Photodetectors Obtaining an External Quantum Efficiency of 37500%. *ACS Appl. Mater. Interfaces* **2015**, *7*, 5890−5897.
(24) Li, G.; Yao, Y.; Yang, H.; Shrotriya, V.; Yang, G.; Yang, Y. ″Solvent Annealing″ Effect in Polymer Solar Cells Based on Poly (3-hexylthiophene) and Methanofullerenes. *Adv. Funct. Mater.* **2007**, *17*, 1636−1644.
(25) Kline, R. J.; Mcgehee, M. D.; Toney, M. F. Highly Oriented Crystals at the Buried Interface in Polythiophene Thin-Film Transistors. *Nat. Mater.* **2006**, *5*, 222−228.
(26) Yang, H. H.; LeFevre, S. W.; Ryu, C. Y.; Bao, Z. N. Solubility-Driven Thin Film Structures of Regioregular Poly(3-hexyl thiophene) Using Volatile Solvents. *Appl. Phys. Lett.* **2007**, *90*, 172116.
(27) Lilliu, S.; Agostinelli, T.; Pires, E.; Hampton, M.; Nelson, J.; Macdonald, J. E. Dynamics of Crystallization and Disorder during Annealing of P3HT/PCBM Bulk Heterojunctions. *Macromolecules* **2011**, *44*, 2725−2734.
(28) Brinkmann, M. Structure and Morphology Control in Thin Films of Regioregular Poly(3-hexylthiophene). *J. Polym. Sci., Part B: Polym. Phys.* **2011**, *49*, 1218−1233.
(29) Chueh, C. C.; Yao, K.; Yip, H. L.; Chang, C. Y.; Xu, Y. X.; Chen, K. S.; Li, C. Z.; Liu, P.; Huang, F.; Chen, Y. W.; Chen, W. C.; Jen, A. K. Y. Non-Halogenated Solvents for Environmentally Friendly Processing of High-Performance Bulk-Heterojunction Polymer Solar Cells. *Energy Environ. Sci.* **2013**, *6*, 3241−3248.
(30) Loiudice, A.; Rizzo, A.; Latini, G.; Nobile, C.; de Giorgi, M.; Gigli, G. Graded Vertical Phase Separation of Donor/Acceptor Species for Polymer Solar Cells. *Sol. Energy Mater. Sol. Cells* **2012**, *100*, 147−152.
(31) Wang, W. B.; Zhang, F. J.; Li, L. L.; Zhang, M.; An, Q. S.; Wang, J.; Sun, Q. Q. Highly sensitive polymer photodetectors with a broad spectral response range from UV light to the near infrared region. *J. Mater. Chem. C* **2015**, *3*, 7386−7393.
(32) Kiriy, N.; Jahne, E.; Adler, H. J.; Schneider, M.; Kiriy, A.; Gorodyska, G.; Minko, S.; Jehnichen, D.; Simon, P.; Fokin, A. A.; Stamm, M. One-Dimensional Aggregation of Regioregular Polyalkylthiophenes. *Nano Lett.* **2003**, *3*, 707−712.
(33) Gurau, M. C.; Delongchamp, D. M.; Vogel, B. M.; Lin, E. K.; Fischer, D. A.; Sambasivan, S.; Richter, L. J. Measuring Molecular Order in Poly(3-alkylthiophene) Thin Films with Polarizing Spectroscopies. *Langmuir* **2007**, *23*, 834−842.
(34) Li, L. G.; Lu, G. H.; Yang, X. N. Improving Performance of Polymer Photovoltaic Devices Using an Annealing-Free Approach via Construction of Ordered Aggregates in Solution. *J. Mater. Chem.* **2008**, *18*, 1984−1990.
(35) Zhang, F. J.; Zhuo, Z. L.; Zhang, J.; Wang, X.; Xu, X. W.; Wang, Z. X.; Xin, Y. S.; Wang, J.; Wang, J.; Tang, W. H.; Xu, Z.; Wang, Y. S. Influence of PC60BM or PC70BM as Electron Acceptor on the Performance of Polymer Solar Cells. *Sol. Energy Mater. Sol. Cells* **2012**, *97*, 71−77.
(36) Xu, X. W.; Zhang, F. J.; Zhang, J.; Wang, H.; Zhuo, Z. L.; Liu, Y.; Wang, J.; Wang, Z. X.; Xu, Z. High Efficient Inverted Polymer Solar Cells with Different Annealing Treatment. *Mater. Sci. Eng., C* **2012**, *32*, 685−691.
(37) Li, Y.; Huang, H. H.; Wang, M. J.; Nie, W. Y.; Huang, W. X.; Fang, G. J.; Carroll, D. L. Spectral Response of Fiber-Based Organic Photovoltaics. *Sol. Energy Mater. Sol. Cells* **2012**, *98*, 273−276.
(38) Cha, H.; Chung, D. S.; Bae, S. Y.; Lee, M. J.; An, T. K.; Hwang, J.; Kim, K. H.; Kim, Y. H.; Choi, D. H.; Park, C. E. Complementary Absorbing Star-Shaped Small Molecules for the Preparation of Ternary Cascade Energy Structures in Organic Photovoltaic Cells. *Adv. Funct. Mater.* **2013**, *23*, 1556−1565.
(39) Malliaras, G.; Salem, J.; Brock, P.; Scott, C. Electrical Characteristics and Efficiency of Single-Layer Organic Light-Emitting Diodes. *Phys. Rev. B: Condens. Matter Mater. Phys.* **1998**, *58*, R13411.
(40) Campbell, I. H.; Crone, B. K. Bulk Photoconductive Gain in Poly(phenylene vinylene) Based Diodes. *J. Appl. Phys.* **2007**, *101*, 024502.
(41) Li, J. H.; Sun, Z. H.; Yan, F. Solution Processable Low-Voltage Organic Thin Film Transistors with High-k Relaxor Ferroelectric Polymer as Gate Insulator. *Adv. Mater.* **2012**, *24*, 88−93.
(42) Yang, H. C.; Shin, T. J.; Yang, L.; Cho, K.; Ryu, C. Y.; Bao, Z. N. Effect of Mesoscale Crystalline Structure on the Field-Effect Mobility of Regioregular Poly(3-hexyl thiophene) in Thin-Film Transistors. *Adv. Funct. Mater.* **2005**, *15*, 671−676.
(43) Chang, J. F.; Sun, B. Q.; Breiby, D. W.; Nielsen, M. M.; Solling, T. I.; Giles, M.; McCulloch, I.; Sirringhaus, H. Enhanced Mobility of Poly(3-hexylthiophene) Transistors by Spin-Coating From High-Boiling-Point Solvents. *Chem. Mater.* **2004**, *16*, 4772−4776.
(44) Sirringhaus, H.; Brown, P. J.; Friend, R. H.; Nielsen, M. M.; Bechgaard, K.; Langeveld-Voss, B. M. W.; Spiering, A. J. H.; Janssen, R. A. J.; Meijer, E. W.; Herwig, P.; de Leeuw, D. M. Two-Dimensional Charge Transport in Self-Organized, High-Mobility Conjugated Polymers. *Nature* **1999**, *401*, 685−688.
(45) Kim, Y.; Cook, S.; Tuladhar, S. M.; Choulis, S. A.; Nelson, J.; Durrant, J. R.; Bradley, D. D. C.; Giles, M.; Mcculloch, I.; Ha, C. S.; Ree, M. A Strong Regioregularity Effect in Self-Organizing Conjugated Polymer Films and High-Efficiency Polythiophene: Fullerene Solar Cells. *Nat. Mater.* **2006**, *5*, 197−203.
(46) Tumbleston, J. R.; Collins, B. A.; Yang, L.; Stuart, A. C.; Gann, E.; Ma, W.; You, W.; Ade, H. The Influence of Molecular Orientation on Organic Bulk Heterojunction Solar Cells. *Nat. Photonics* **2014**, *8*, 385−391.
(47) Dou, L. T.; Yang, Y.; You, J. B.; Hong, Z. R.; Chang, W. H.; Li, G.; Yang, Y. Solution-Processed Hybrid Perovskite Photodetectors with High Detectivity. *Nat. Commun.* **2014**, *5*, 5404.

DOI: 10.1021/acsami.5b07522
ACS Appl. Mater. Interfaces 2015, 7, 22660−22668